J. Fluid Mech. (1980), *vol.* 99, *part* 1, *pp.* 163–183
Printed in Great Britain

A parametrical model for the vertical structure of the induced atmospheric pressure field above a spectrum of surface gravity waves

By ROBERT BRYAN LONG

Sea–Air Interaction Laboratory, Atlantic Oceanographic and Meteorological Laboratories, National Oceanic and Atmospheric Administration, Miami, Florida

(Received 12 December 1978 and in revised form 14 November 1979)

A useful parametrical model for the vertical structure of the pressure field induced by wind blowing over a field of surface gravity waves is proposed. The model is a linear expansion in a set of empirical orthogonal functions, derived from a set of 110 complex pressure profiles computed according to the theory of Miles (1957), and provides a compact, quantitative description of those profiles. The model has been used as an element in the analysis of a body of experimental data on wave-induced atmospheric pressure fluctuations obtained by Snyder *et al.* (1980).

1. Introduction

The primary mechanism for the transfer of energy and momentum from the wind to gravity waves on the surface of a body of water is the working of atmospheric pressure fluctuations on the moving water surface. These pressure fluctuations are composed of two parts, a turbulent component and a component induced by the wind blowing over the wavy surface. The latter part dominates the atmospheric input to the wave field except for wave components with essentially negligible energy densities. The objective of the present work is to develop a useful parametrical model for the vertical structure of this wave-induced component of the pressure field; as a by-product of that development, we have produced a detailed picture of the theoretical wave-induced pressure field according to Miles (1957). This undertaking was motivated by the following considerations.

It is easily shown that the spectral quantity defining the rate at which wave-coherent pressure fluctuations do work on the wave field is the surface-displacement/atmospheric-pressure directional cross-spectrum, $E_{\zeta P}(\theta, \omega; z)$, where ζ is surface displacement, P is atmospheric pressure, ω and θ are wave radian frequency and vector wavenumber direction respectively, and z is the elevation relative to the mean water surface at which the pressure is defined. We may, for example, expand the two fields in Fourier–Stieltjes integrals,

$$\zeta(\mathbf{x}, t) = \int_{\mathbf{k}} \int_{\omega} d\zeta(\mathbf{k}, \omega)\, e^{i(\mathbf{k}\cdot\mathbf{x}-\omega t)},$$

$$P(\mathbf{x}, z, t) = \int_{\mathbf{k}} \int_{\omega} dP(\mathbf{k}, \omega; z)\, e^{i(\mathbf{k}\cdot\mathbf{x}-\omega t)},$$

0022-1120/80/4472-1190 $02.00

where $d\zeta(\mathbf{k}, \omega)$ and $dP(\mathbf{k}, \omega; z)$ are the complex differential amplitudes of the respective fields at horizontal vector wavenumber $\mathbf{k}$ and frequency ω, $\mathbf{x}$ is a horizontal position vector, and t is time. The average rate of energy transfer per unit horizontal area from wind to waves is, to lowest order,

$$w = \left\langle -\frac{\partial \zeta}{\partial t}(\mathbf{x}, t)\, P(\mathbf{x}, 0, t) \right\rangle,$$

where $\langle\,\rangle$ indicates ensemble average. Substituting the expansions into this expression and invoking linear gravity wave dispersion and the reality, homogeneity, and stationarity of the two fields, we get, after some simple manipulations,

$$w = -2\int_0^{2\pi} d\theta \int_0^{\infty} d\omega\, \omega\, \mathrm{Im}\{E_{\zeta P}(\theta, \omega; 0)\},$$

where

$$E_{\zeta P} = \frac{\langle d\zeta\, dP^* \rangle}{d\theta\, d\omega} \tag{1.1}$$

(the asterisk indicating complex conjugate).

Thus, at the small wave-amplitude limit, $E_{\zeta P}(\theta, \omega; z)$ evaluated at the mean water surface ($z = 0$) fixes the atmospheric energy flux into the corresponding wave component. At the same level of approximation, the wave-coherent pressure fluctuations represent a linear response of the air flow to the boundary perturbations caused by the surface waves; consequently, we can write

$$dP(\theta, \omega; z) = \hat{P}(\theta, \omega; z)\, d\zeta(\theta, \omega),$$

where $\hat{P}$ is a complex function defining the vertical structure of the wave-induced pressure field. Using this in (1.1) gives

$$E_{\zeta P} = \hat{P}^* E_{\zeta^2}, \tag{1.2}$$

where

$$E_{\zeta^2} = \frac{\langle d\zeta\, d\zeta^* \rangle}{d\theta\, d\omega}$$

defines the surface-wave directional spectrum.

Field experiments designed to measure $E_{\zeta P}$ typically employ an array of air pressure probes, distributed vertically and/or horizontally, superposed on a horizontal array of wave gauges. As few as one instrument of each type (Dobson 1971) and as many as seven pressure sensors and six wave gauges (Snyder *et al.* 1980) have been used. Spectral analysis of the resulting time series provides frequency cross-spectra between surface elevation at a number of horizontal displacements, between atmospheric pressure at a number of heights and displacements in the horizontal, and between surface elevation and atmospheric pressure at a number of heights and horizontal displacements. These data represent integral properties of E_{ζ^2}, $E_{\zeta P}$, and the three-dimensional atmospheric pressure spectrum (F_{Q^2} in the notation of Snyder *et al.*). In particular,

$$G_{\zeta P}(\omega; \mathbf{r}, z) = \int_0^{2\pi} d\theta\, E_{\zeta P}(\theta, \omega; z)\, e^{-\mathbf{k}(\omega, \theta)\cdot \mathbf{r}} \tag{1.3}$$

defines the frequency cross-spectrum between surface elevation and atmospheric pressure at height z and horizontal displacement $\mathbf{r}$. In order to extract an estimate of

$E_{\zeta P}$ from such a data set, it is necessary to construct parametrical models of E_{ζ^2} and the pressure transfer function $\hat{P}$ to be fitted in the least-squares sense to the observed set of frequency cross-spectra. Because of the limited number of discrete horizontal displacements and vertical positions provided by the instrument array and the statistical variability present in the observations, the number of free parameters in the models must be severely constrained to assure statistically significant results. It is important, therefore, to use any available *a priori* knowledge (or intuition, if necessary) to design parametrical models which are efficient at representing the respective fields.

A variety of models for the directional properties of E_{ζ^2} and $\hat{P}$ has been applied in the past, ranging in complexity from the unidirectional distributions implicitly assumed by Dobson (1971) and Elliott (1972) to the bilinear expansions of Snyder (1974). Models for the vertical structure of $\hat{P}$ have generally assumed, in analogy with potential flow (uniform mean wind profile) theory, that the wave-induced pressure decays as e^{-bkz}; Snyder took $b = 1$, while Elliott allowed b to be a free parameter, fixed in the course of his analysis. The much more extensive data set of Snyder *et al.* (1980) allowed the application of more flexible vertical structure models, several of which were, in fact, used. Each took the form of a linear or bilinear expansion in one of two sets of z-dependent basis functions. The present work focuses on the derivation of one of these sets, founded in this case not on analogy with potential flow, but instead on the hypothesis that a parametrical model yielding an optimal representation of the pressure profiles predicted by Miles' theory will be nearly optimal for representing those existing in nature.

Accordingly, 110 complex pressure profiles have been computed from Miles' governing equations for a range of wind and wave parameters (§ 2); these were then subjected to empirical orthogonal function analysis to identify the dominant modes of vertical dependence in the profile set (§ 3). A linear expansion in the four dominant empirical orthogonal functions proved capable of representing 99·9999% of the variance about zero of the theoretical profile set and is the optimal linear expansion of these profiles (in the sense that no other four-parameter expansion can approximate the profiles with a smaller residual mean square error). Contour plots of the four complex coefficients, along with the empirical orthogonal functions themselves, provide a graphical description of the wave-induced pressure field according to Miles. To the extent that nature differs from theory, a linear expansion in the same set of basis functions may be less than optimal for representing real profiles but is likely, nevertheless, to be more efficient than any model based on some arbitrarily selected basis function set or on less relevant *a priori* notions about the vertical structure of the wave-induced pressure field.

2. The structure of the wave-induced pressure field according to Miles

Central to our present understanding, albeit limited, of the pressure field induced by a sheared wind blowing over propagating surface waves is the theory of Miles (1957). It has the nice advantage of mathematical rigour, although the simplifications invoked to make the problem tractable result in a number of physically unrealistic consequences. In particular, the neglect of viscosity and the perturbation turbulent

Reynolds stresses in the theory results in the appearance of an integrable singularity in the wave-induced velocity field at the critical height (the elevation above the mean surface where the mean wind speed matches the wave phase speed); this, in turn, causes the wave growth rate to depend rather sensitively on the properties of the mean wind profile at that level. Nevertheless, most subsequent efforts to improve on Miles' formulation by including one or more of the factors neglected in his theory did not find that the resulting wave growth rates differed radically from Miles' calculations (Phillips 1966; Hasselmann 1967, 1968; Davis 1969, 1970; Townsend 1971; Gent & Taylor 1976). Although the field experiments of Dobson (1971) indicated growth rates an order of magnitude larger than Miles predicts, later work (Elliott 1972; Snyder 1974; Snyder *et al.* 1980) has shown that the discrepancy is considerably less than this, perhaps no more than a factor of 2. These developments suggest that, despite its shortcomings, Miles' theory may still represent a useful asymptotic approximation and that smoothed properties of his model, such as pressure profiles, may indeed exhibit the dominant characteristics of those existing in nature. For that reason, as well as for its tractability and self-sufficiency, we deem Miles' theory to be suitable for our purpose here.

Miles considered the effect on a basic shear flow (the wind) of a perturbation caused by a small amplitude surface wave running along x at an angle θ with respect to the wind direction. The component of the wind profile along x was taken to be (outside a thin, viscous sublayer)

$$U(z) = U_1 \ln\left(\frac{z}{z_0}\right),$$

where

$$U_1 = \frac{U_*}{\kappa}\cos\theta,$$

typical of the near-surface turbulent atmospheric boundary layer; U_* is the friction velocity, κ is von Kármán's constant ($= 0{\cdot}4$), z_0 is the roughness length, and z is the vertical co-ordinate measured upward from the mean sea surface. Neglecting viscosity and the perturbation turbulent Reynolds stresses, the linearized equations of motion governing the small perturbation in the air flow are

$$\left.\begin{aligned} \rho(u_t + Uu_x + wU_z) &= -P_x, \\ \rho(w_t + Uw_x) &= -P_z, \\ u_x + w_z &= 0, \end{aligned}\right\} \tag{2.1}$$

with boundary conditions

$$w = \zeta_t + U(0)\zeta_x \quad \text{on} \quad z = 0,$$

$$u = w = 0 \quad \text{as} \quad z \to \infty,$$

where ζ is the sea surface elevation, ρ is the density of air, P the wave-induced pressure, u and w are the x and z components of wave-induced velocity, respectively, and t is time. The subscripts denote partial differentiation with respect to the indicated variable. The surface wave is introduced by setting

$$\zeta = d\zeta e^{ik(x-Ct)},$$

where k is the surface wavenumber and C its phase velocity. Introducing a stream function Ψ to represent u and w satisfies the third of equations (2.1) exactly. Then, letting

$$\Psi = \hat{\Psi}(z)\, d\zeta\, e^{ik(x-Ct)},$$

and

$$P = \hat{P}(z)\, d\zeta\, e^{ik(x-Ct)},$$

in the first two of (2.1) gives

$$(U-C)(\hat{\Psi}_{zz} - k^2\hat{\Psi}) - U_{zz}\hat{\Psi} = 0 \tag{2.2}$$

governing the vertical structure of the flow, with

$$\hat{\Psi} = C - U(0) \quad \text{on} \quad z = 0,$$
$$\hat{\Psi} = 0 \quad \text{as} \quad z \to \infty \tag{2.3}$$

for boundary conditions. The pressure vertical structure is given either by

$$\hat{P}(z) = \rho(U_z\hat{\Psi} - (U-C)\hat{\Psi}_z),$$

or

$$\hat{P}(z) = \rho k^2 \int_z^\infty dz\,(U-C)\hat{\Psi}, \tag{2.4}$$

the second of which is preferred if solutions must be obtained numerically, as is the case here. The $\hat{\Psi}$ and $\hat{P}$ profiles are, of course, implicitly dependent on the parameters of the wind (U_1 and z_0) and the wave (ω, which fixes k and C through the dispersion relation); for simplicity here, we have explicitly indicated only the dependence on z.

Equation (2.2) is the well-known Rayleigh equation of hydrodynamical stability theory. It is singular at the critical height $z = z_c$, where $U(z_c) = C$. As a consequence, one of its two independent solutions has a logarithmic branch point there, and the question of the correct representation of the solution for $z < z_c$ reduces to whether it should be joined to the solution for $z > z_c$ via an infinitesimal indentation in the complex-z plane passing above or below the singularity. In either case, $\hat{\Psi}$ is continuous across the critical height, but all its derivatives (and, hence, u also) diverge there. By considering a thin, viscous layer centred on $z = z_c$, this non-physical behaviour is removed and the proper connexion identified as the indentation under the singular point (see, for example, Meksyn 1961; Lin 1967; Long 1971).

With minor modifications, the system of equations (2.2) and (2.3) are the ones solved numerically by Conte & Miles (1959) to obtain values of Miles' growth rate parameter β, defined in the present notation by

$$\hat{P}(0) = U_1^2 \rho k(\alpha + i\beta). \tag{2.5}$$

The modifications included (*a*) transformation to $U(z)$, instead of z, as the independent variable, (*b*) applying the lower boundary condition at $z = z_0\,(U = 0)$, instead of $z = 0$, (*c*) replacing the boundary condition at infinity by

$$\hat{\Psi}_z + k\hat{\Psi} = 0 \quad \text{as} \quad U \to \infty,$$

equivalent to requiring $\hat{\Psi}$ to decay as e^{-kz} for large z, and (*d*) non-dimensionalizing using U_1 and $1/k$ as velocity and length scales. The resulting equations were solved numerically by a fourth-order Runge–Kutta procedure. Starting values of each of the two independent solutions, $\hat{\Psi}_1$ and $\hat{\Psi}_2$, and their derivatives just above and just below

the singular point were derived from truncated versions of the analytical power series solutions, obtainable by the method of Frobenius. The two solutions were then integrated separately down to $U = 0$ ($z = z_0$), then upward (from the starting points near $U = C$ ($z = z_c$)), pausing periodically to apply the boundary conditions and fix the coefficients in the full solution

$$\hat{\Psi} = A\hat{\Psi}_1 + B\hat{\Psi}_2.$$

The upward integration was stopped whenever the values of A and B stabilized. Although the $\hat{\Psi}_1$ and $\hat{\Psi}_2$ often diverged as U (or z) increased, stable A and B values were always obtained before machine overflow occurred.

Conte & Miles report only the parameters α and β, defined by (2.5), and provide no other information on the pressure vertical structure. For our purpose now, it is necessary to resolve the system (2.2), (2.3), and (2.4) to obtain $\hat{P}(z)$ profiles for a reasonably broad range of wind and wave parameters. To do this, a different numerical procedure was implemented, possibly slightly less accurate than the technique of Conte & Miles but much more conservative of computer time and much easier to apply. We describe this procedure briefly below.

First, we modified equations (2.2), (2.3), and (2.4) as Conte & Miles did (steps (*a*)–(*d*) above). We generalized the new vertical co-ordinate $U' = \ln(z'/z'_0)$ (primes indicating dimensionless quantities) to allow it to take on complex values, then chose a curved path in the complex-U' plane which passed below the singularity at $U' = C'$ and terminated at $U' = 0$ and $U' = U'_b$, where boundary conditions are to be applied (for all calculations reported here, U_b was the wind speed two surface wavelengths above the mean water level). The differential equation was replaced by a central finite-difference approximation defined on a mesh of 199 points equally spaced along the curved path. This formulation led to a system of linear algebraic equations for the 199 complex $\hat{\Psi}'$ values at the mesh points. Although the coefficient matrix was 199×199, only 5 elements (at most) of each row were non-zero, so that solving the matrix problem was easy and uncomplicated. The use of U' (rather than z') for the vertical co-ordinate causes the mesh points to be densely distributed close to the surface, where most of the variability in the solution is expected, and to be spread more thinly higher up in the flow, where the behaviour of the solution is expected to be simple ($\sim e^{-z'}$). The pressure along the curved path was then computed by inserting the $\hat{\Psi}'$ solution into the non-dimensional version of (2.4) and integrating numerically. Finally, this result was extrapolated by analytic continuation onto the real-U' axis. Since our curved solution path and that of Conte & Miles (including their infinitesimal indentation under $U' = C'$) lie in the same simply connected region within which all functions involved are analytic, our analytically continued solution for the pressure on the real axis ought to be, within computational error, the same as theirs, had they computed it.

This procedure has the advantage of complete numerical stability, but it is subject to two sources of error not usually present in this kind of calculation. First, the accuracy of the finite-difference approximations to the various derivatives is somewhat reduced because the several mesh points defining the derivatives are not exactly collinear when the path is curved. This difficulty was minimized by choosing a segment of a circle in the complex-U' plane for the curved path. Second, truncation error

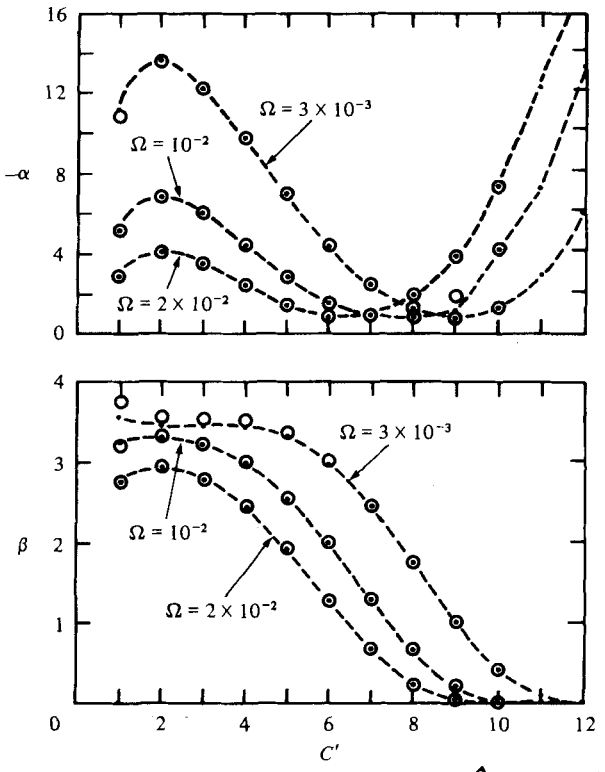

FIGURE 1. Comparison between real and imaginary parts of $\hat{P}' = \alpha + i\beta$ at $z = 0$ as computed here (○) and as computed by Conte & Miles (1959) (– – · – –).

becomes very large if the path passes too close to the singularity, where all the derivatives of $\hat{\Psi}''$ diverge. Minimizing the former error calls for a large path radius of curvature, but this worsens the error due to the second source. We have experimentally determined an acceptable compromise between these conflicting difficulties by solving the problem repeatedly for one set of wind/wave parameters, readjusting the path curvature after each trial, until the differences between our α and β values and those of Conte & Miles were approximately minimized. The same path was then used on all subsequent calculations. A comparison between Conte & Miles results and ours is shown in figure 1. The two parameters of the problem are $C' = C/U_1$ and Miles' wind profile parameter

$$\Omega = gz_0/U_1^2.$$

Deep water dispersion has been assumed. Agreement is generally excellent between the two calculations. The largest discrepancies are for $C' = 1$ and $\Omega = 3 \times 10^{-3}$ and at $C' = 9$ and $\Omega = 10^{-2}$. We suspect that, in the latter case at least, our value is more accurate than theirs, since theirs causes the corresponding curve to be somewhat kinked at this point.

To test the analytic continuation procedure for extrapolating the curved path solution onto the real axis, the problem was solved for a uniform wind profile (but retaining the log profile as the independent co-ordinate replacing z in the numerical

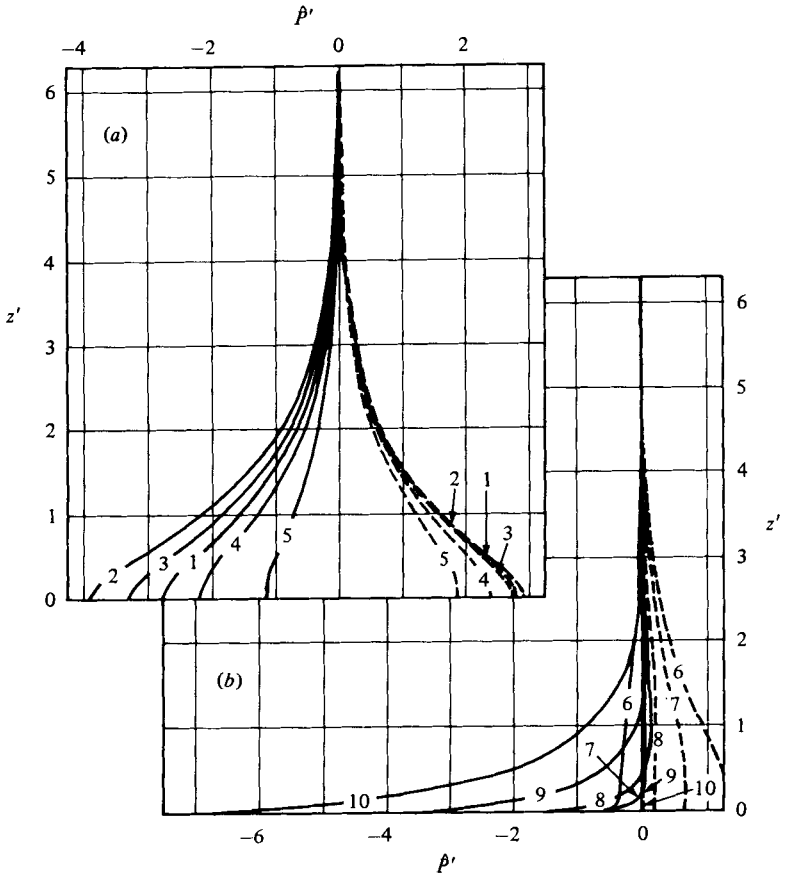

FIGURE 2. $\hat{P}'$ profiles, computed from Miles' (1957) theory, plotted *versus* dimensionless height $z' = kz$ for $\Omega = 0{\cdot}021$. Solid curves are $\alpha = \mathrm{Re}\{\hat{P}'\}$, dashed curves are $\beta = \mathrm{Im}\{\hat{P}'\}$. Profiles for $C' = C/U_1 = 1$ to 5 are shown in (*a*), 6 to 10 in (*b*).

procedure). The system of equations (2.2), (2.3), and (2.4) can be solved exactly for this case, giving (in dimensional form)

$$\hat{P}(z) = -\rho k(U-C)^2 e^{-kz}.$$

The analytically continued numerical solution (for $U' = 6{\cdot}2$, $C' = 3{\cdot}0$) agreed with the exact solution to within 5·2 % in magnitude and 0·5° in phase at all elevations (up to 2 wavelengths) in the flow. For all elevations below 1 wavelength, no error exceeded 1·8 % in magnitude or 0·4° in phase.

The procedure was used to compute theoretical pressure profiles for eleven equally spaced values of Ω on the interval 0·001–0·021 and for C' values ranging from 1 to 10 in steps of 1. The profiles for $\Omega = 0{\cdot}021$ are shown in figures 2 and 3. Here, we have generalized Miles' α and β parameters (equation (2.5)) to be z dependent, viz.

$$\alpha(z)+i\beta(z) \equiv \left(\frac{1}{U_1}\right)^2 \frac{1}{\rho k}\hat{P}(z) = \hat{P}'(z).$$

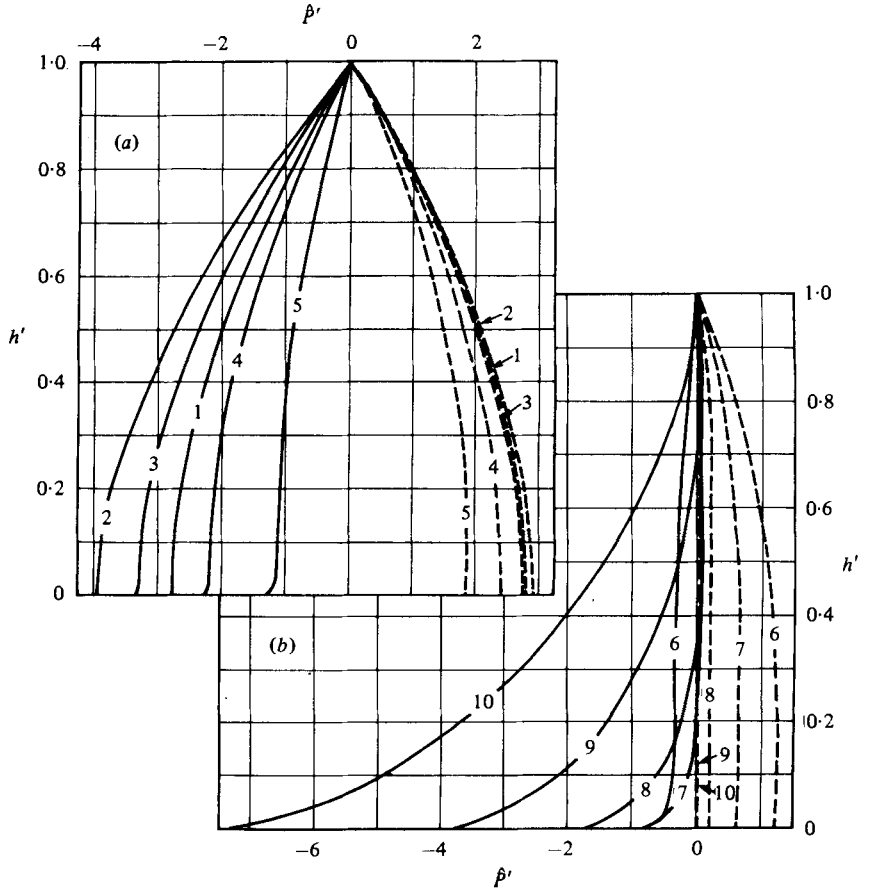

FIGURE 3. Same profiles as in figure 2 but plotted versus $h' = 1-e^{-z'}$. Note that the corresponding model profiles using four empirical orthogonal functions (see § 3) are indistinguishable on this scale from the curves shown.

In terms of the dimensionless variables in which the numerical calculations were actually carried out, this is easily shown to be given by

$$\alpha(z')+i\beta(z') = \int_{z'}^{\infty} dz'\,(U'-C')\,\hat{\Psi}',$$

where $z' = kz$, $U' = U/U_1$, $C' = C/U_1$, and $\hat{\Psi}' = U_1^{-1}\hat{\Psi}$. Figure 2 shows α and β for $\Omega = 0{\cdot}021$ in the interval from the surface to $z' = 2\pi$ (one wavelength above the surface). Most of the variability in the profiles is clearly confined to the region near the surface. In figure 3, the same profiles are plotted versus a deformed vertical co-ordinate,

$$h' = 1-e^{-z'}.$$

This representation has several advantages, e.g. the entire range of elevations $0 \leqslant z \leqslant \infty$ corresponds to $0 \leqslant h' \leqslant 1$; moreover, the region near the surface is stretched out while that higher in the flow is compressed, so that the structure in the solutions is more evenly distributed over the plots. (The co-ordinate U' in which the calculations

were actually performed also has this second advantage but does not serve as well for the presentation of results because the domain of the numerical solutions, $0 < z' < 4\pi$, maps into a different domain in U' for every combination of Ω and C'.) Finally, the function $e^{-z'}$ (the expected vertical dependence of $\hat{P}'$ for a uniform wind profile) maps into a straight line,

$$e^{-z'} = 1 - h'$$

in this representation. Thus, the extent to which a theoretical profile deviates from a straight line when plotted versus h' is an indication of the extent to which the sheared wind profile solution deviates from the uniform profile case.

For smaller Ω values, the development of the α and β profiles with increasing C' was found to be qualitatively similar to that shown here for $\Omega = 0{\cdot}021$ except that development progressed more slowly with increasing C' as Ω was reduced. This similarity of profile development suggested that the theoretical results could be compressed very efficiently by applying the method of empirical orthogonal functions to the set of computed profiles. This procedure has been frequently used to interpret observational data (see, for example, Winant, Inman & Nordstrom 1975; Smith & Woolf 1976; Davis 1976), but it serves equally well for numerically generated theoretical data sets such as we have here. Moreover, it leads to a mathematically convenient model for the experimentally measured pressure field, viz.

$$\hat{P}(z)_{\text{observed}} = \sum_j a_j \phi_j(kz), \tag{2.6}$$

i.e. a linear expansion in the empirical orthogonal functions of the theoretical profile set. To whatever extent the observations resemble theory, this model is the optimal linear expansion, promising an accurate representation with a minimum number of free parameters a_j.

3. Empirical orthogonal functions for Miles' pressure profiles

The method of empirical orthogonal functions is developed in detail elsewhere (see, for example, Lorenz 1956; Moore 1974). In the present application, it proceeds as follows.

We have already noted the qualitative similarities among the 110 pressure profiles computed from Miles' theory; this degree of similarity, in fact, extends to both real and imaginary parts. Consequently, all 220 α and β profiles were interpolated to 50 standard elevations in the co-ordinate $h' = 1 - e^{-z'}$ ranging from 0 to 0·99999 ($z \approx 1{\cdot}8$ wavelengths up into the flow), then assembled into a 50×220 'data' matrix $\mathbf{Q}$. The 50×50 'covariance' matrix $\mathbf{Q}\mathbf{Q}^T$ was then computed. The eigenvectors of this matrix are the optimal basis function set for modelling the pressure profiles forming $\mathbf{Q}$. Specifically, if we assemble the J eigenvectors ϕ_j with the largest eigenvalues into a $50 \times J$ matrix $\mathbf{\Phi}$, we may write

$$\mathbf{Q} = \mathbf{\Phi}\mathbf{A} + \mathbf{R},$$

where $\mathbf{A}$ is a coefficient matrix and $\mathbf{R}$ the matrix of residuals not representable by (i.e. orthogonal to) the eigenvectors in $\mathbf{\Phi}$. It can be shown that no other choice for $\mathbf{\Phi}$ having the same dimensions can produce a smaller residual (i.e. a smaller Euclidian

No.	Eigenvalue	% of total variance
1	$9{\cdot}9060 \times 10^{4}$	99·4744
2	$5{\cdot}0573 \times 10^{2}$	0·5078
3	$1{\cdot}6744 \times 10$	0·0168
4	$8{\cdot}4046 \times 10^{-1}$	0·0008
5	$9{\cdot}8968 \times 10^{-2}$	0·0001

TABLE 1. Eigenvalues of the Miles pressure profiles covariance matrix

norm $\|\mathbf{R}\|_2$, which is just the sum of the squared errors in the model representation $\mathbf{\Phi A}$ of $\mathbf{Q}$). Moreover, if $\mathbf{\Phi}$ includes all of the eigenvectors with non-zero eigenvalues, $\mathbf{Q}$ can be represented exactly ($\mathbf{R}$ vanishes). Finally, each eigenvalue is proportional to the fraction of the variance of the entire data set representable by the corresponding eigenvector (which is why $\mathbf{\Phi}$ was constructed with the J eigenvectors with largest eigenvalues). The five largest eigenvalues of $\mathbf{QQ}^T$ are shown in table 1. Clearly, the successive eigenvalues are converging on zero so rapidly that additional eigenvectors are totally unnecessary to adequately represent the data. We can, in fact, model 99·9999 % of the variance in the whole data set using only the first four eigenvectors, and, for the results reported here, $\mathbf{\Phi}$ was composed of these four, normalized so that

$$\mathbf{\Phi}^T\mathbf{\Phi} = \mathbf{I},$$

where $\mathbf{I}$ is the 4×4 identity matrix. The 4×220 coefficient matrix $\mathbf{A}$ is then given by

$$\mathbf{A} = \mathbf{\Phi}^T\mathbf{Q}.$$

The four dominant eigenvectors, numbered in order of descending eigenvalue, are listed in table 2 and shown graphically in figure 4. The fundamental mode, accounting for 99·47 % of the variability about zero of the Miles profile set, is a smooth curve which decays monotonically toward zero at a rate somewhat slower than e^{-kz}. The second mode drops from a positive value at the surface to a negative minimum at about $h' = 0{\cdot}57$ before decaying to zero. Higher modes exhibit increasingly rapid oscillations with z and rapidly diminishing contributions to the variance of the set of theoretical profiles; the third mode contributes 1/30 that of the second, while the contribution from the fourth is 1/635 that of the second (cf. table 1).

The elements of the matrix $\mathbf{A}$ provide the grid of complex coefficient values a_j' contoured in figures 5(*a*)–(*h*). These plots, along with the eigenfunctions shown in figure 4 and table 2, summarize the theoretical wave-induced pressure calculations according to Miles for this domain of parameters. Note that the fundamental mode ϕ_1 dominates the pressure profile shapes over much of the (C', Ω) plane, the topography of a_1' being typically an order of magnitude (or more) larger than that of a_2', a_3', and a_4'. Hence, pressure profiles for this range of parameters will decay with z, like ϕ_1, more slowly than e^{-kz}. Note also that, as C' and Ω increase, the increasing contribution to the profile shapes of ϕ_2 relative to ϕ_1 tends initially to cancel the curvature in ϕ_1, resulting in a gradual shift toward e^{-kz} dependence. These characteristics are consistent with the observations of Elliott (1972) which indicated a slower-than-e^{-kz} decay of the wave-induced pressure field and a tendency of the decay to shift toward e^{-kz} as the ratio of wave phase speed to wind speed increased. (However, Elliott did not detect

h'	ϕ_1	ϕ_2	ϕ_3	ϕ_4
0	0·2126	0·4728	0·6022	0·4665
0·0204	0·2109	0·3553	0·1939	−0·1248
0·0408	0·2096	0·2861	0·0375	−0·2337
0·0612	0·2081	0·2319	−0·0528	−0·2486
0·0816	0·2063	0·1867	−0·1088	−0·2259
0·1020	0·2042	0·1479	−0·1435	−0·1866
0·1224	0·2019	0·1140	−0·1638	−0·1409
0·1429	0·1995	0·0839	−0·1741	−0·0940
0·1633	0·1968	0·0571	−0·1769	−0·0490
0·1837	0·1940	0·0331	−0·1742	−0·0074
0·2041	0·1911	0·0114	−0·1674	0·0296
0·2245	0·1880	−0·0081	−0·1575	0·0616
0·2449	0·1847	−0·0258	−0·1452	0·0885
0·2653	0·1814	−0·0417	−0·1311	0·1102
0·2857	0·1779	−0·0561	−0·1158	0·1271
0·3061	0·1743	−0·0690	−0·0997	0·1390
0·3265	0·1706	−0·0807	−0·0829	0·1466
0·3469	0·1668	−0·0911	−0·0659	0·1500
0·3673	0·1629	−0·1004	−0·0488	0·1494
0·3878	0·1589	−0·1086	−0·0318	0·1454
0·4082	0·1548	−0·1158	−0·0151	0·1383
0·4286	0·1507	−0·1220	0·0012	0·1285
0·4490	0·1464	−0·1274	0·0170	0·1162
0·4694	0·1421	−0·1318	0·0322	0·1017
0·4898	0·1376	−0·1355	0·0468	0·0855
0·5102	0·1331	−0·1384	0·0605	0·0678
0·5306	0·1285	−0·1405	0·0734	0·0490
0·5510	0·1239	−0·1418	0·0853	0·0294
0·5714	0·1191	−0·1425	0·0963	0·0093
0·5918	0·1143	−0·1424	0·1063	−0·0110
0·6122	0·1094	−0·1417	0·1152	−0·0312
0·6326	0·1045	−0·1403	0·1229	−0·0509
0·6531	0·0994	−0·1383	0·1295	−0·0700
0·6735	0·0943	−0·1357	0·1349	−0·0882
0·6939	0·0891	−0·1324	0·1391	−0·1052
0·7143	0·0838	−0·1285	0·1420	−0·1207
0·7347	0·0785	−0·1240	0·1436	−0·1345
0·7551	0·0731	−0·1189	0·1439	−0·1464
0·7755	0·0676	−0·1132	0·1428	−0·1561
0·7959	0·0620	−0·1068	0·1401	−0·1635
0·8163	0·0563	−0·0998	0·1360	−0·1680
0·8367	0·0506	−0·0922	0·1301	−0·1697
0·8571	0·0447	−0·0839	0·1225	−0·1677
0·8775	0·0388	−0·0749	0·1133	−0·1620
0·8980	0·0327	−0·0652	0·1019	−0·1522
0·9184	0·0266	−0·0547	0·0882	−0·1377
0·9388	0·0203	−0·0432	0·0723	−0·1175
0·9592	0·0138	−0·0307	0·0533	−0·0906
0·9796	0·0071	−0·0168	0·0305	−0·0545
1	0	0	0	0

TABLE 2. Empirical orthogonal functions for Miles' pressure profiles

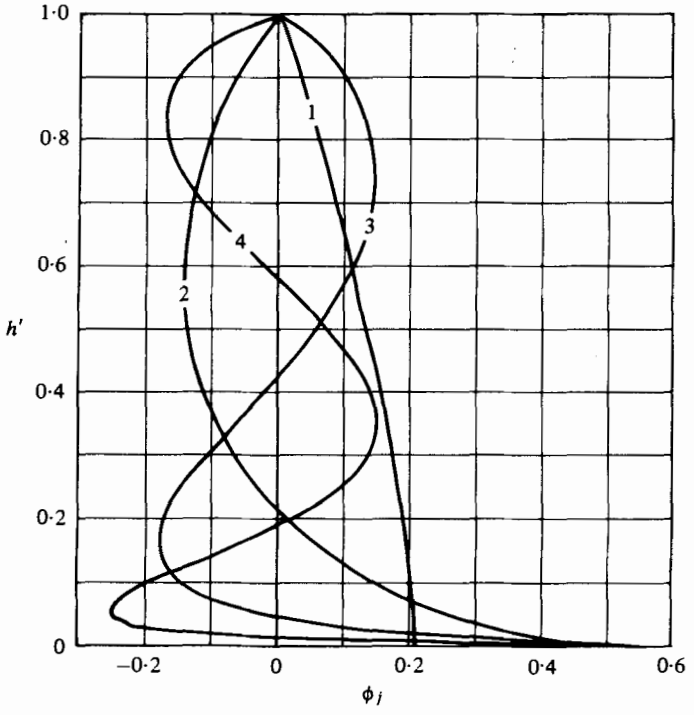

FIGURE 4. Empirical orthogonal functions derived from the pressure profiles computed from Miles' theory. The functions shown are those with the four largest eigenvalues and are ordered according to descending eigenvalue (see table 1).

the faster-than-e^{-kz} decay predicted by the theory for the higher C' and Ω values; see, for example, the profiles of figure 3(*b*) for $C' = 7$, 8, 9 and 10.) It is difficult to make more precise comparisons between Miles' theory and existing field data because the experimental values of the wind profile parameters U_1 and Ω have not been sufficiently well known; determinations of Ω, in particular, are subject to large and erratic fluctuations, presumably due to the sensitivity of this parameter to instrumental and statistical sampling error. Nevertheless, these qualitative agreements with Elliott's observations lend additional support to the notion that a parametrical model based on Miles' theory may be nearly optimal for representing pressure profiles existing in nature.

This hypothesis cannot be tested against real profiles because no direct, model-independent determination of the structure of real, wave-induced pressure profiles has been accomplished; but we have tested the flexibility of the expansion by fitting it to theoretical profiles which are not members of the Miles set, for example one characteristic of potential flow ($\hat{P}' = -e^{-z'}$) and another computed according to the theory of Long (1971). (Long's theory incorporates perturbation turbulent Reynolds stresses using a closure hypothesis similar to Townsend's (1971).) These profiles were well represented by two-term expansions; using four terms, the reconstructions were almost identical with the originals.

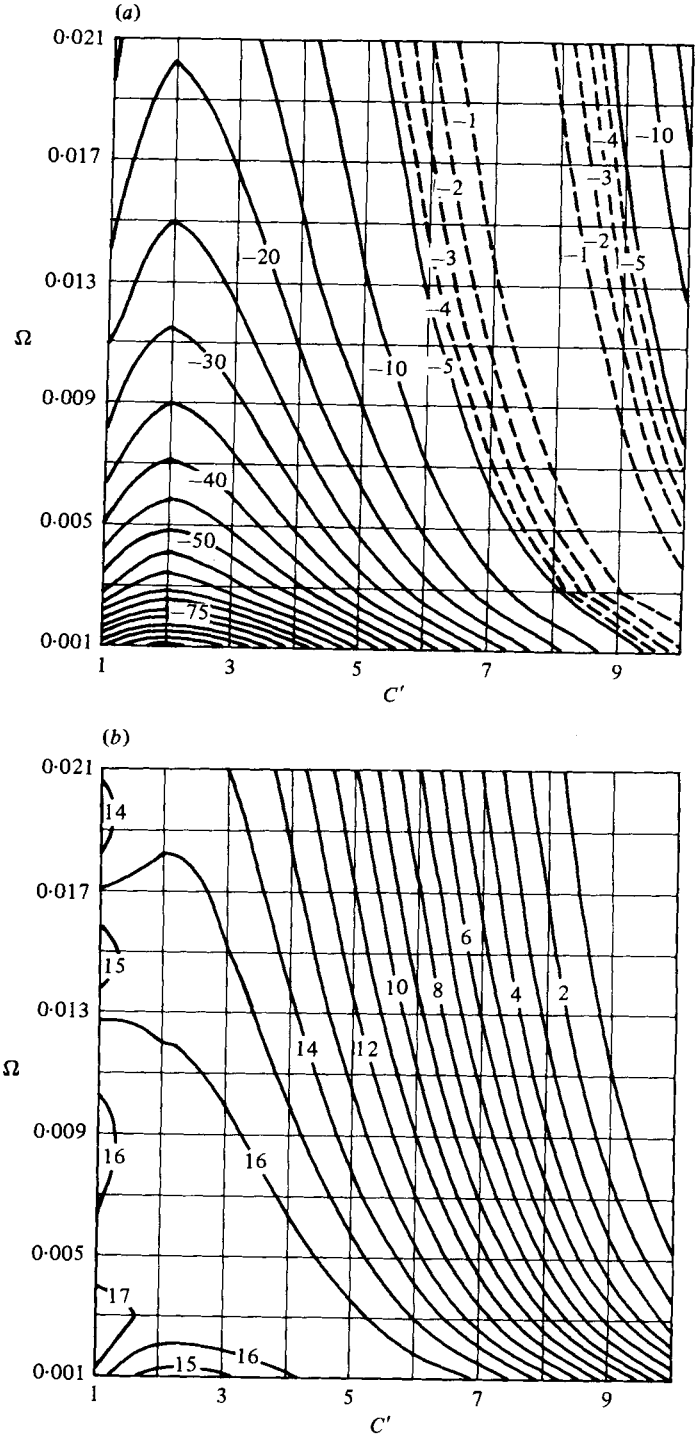

FIGURE 5. For legend see p. 179.

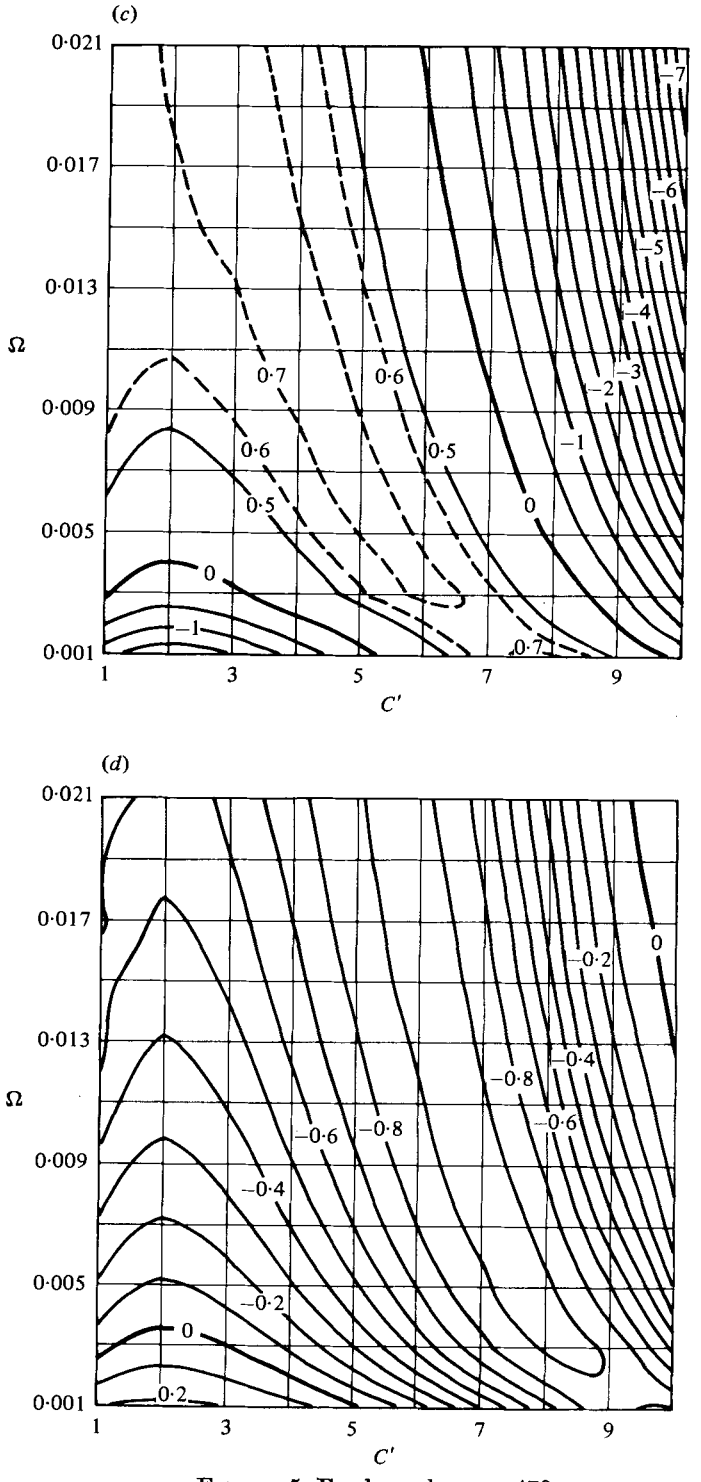

FIGURE 5. For legend see p. 179

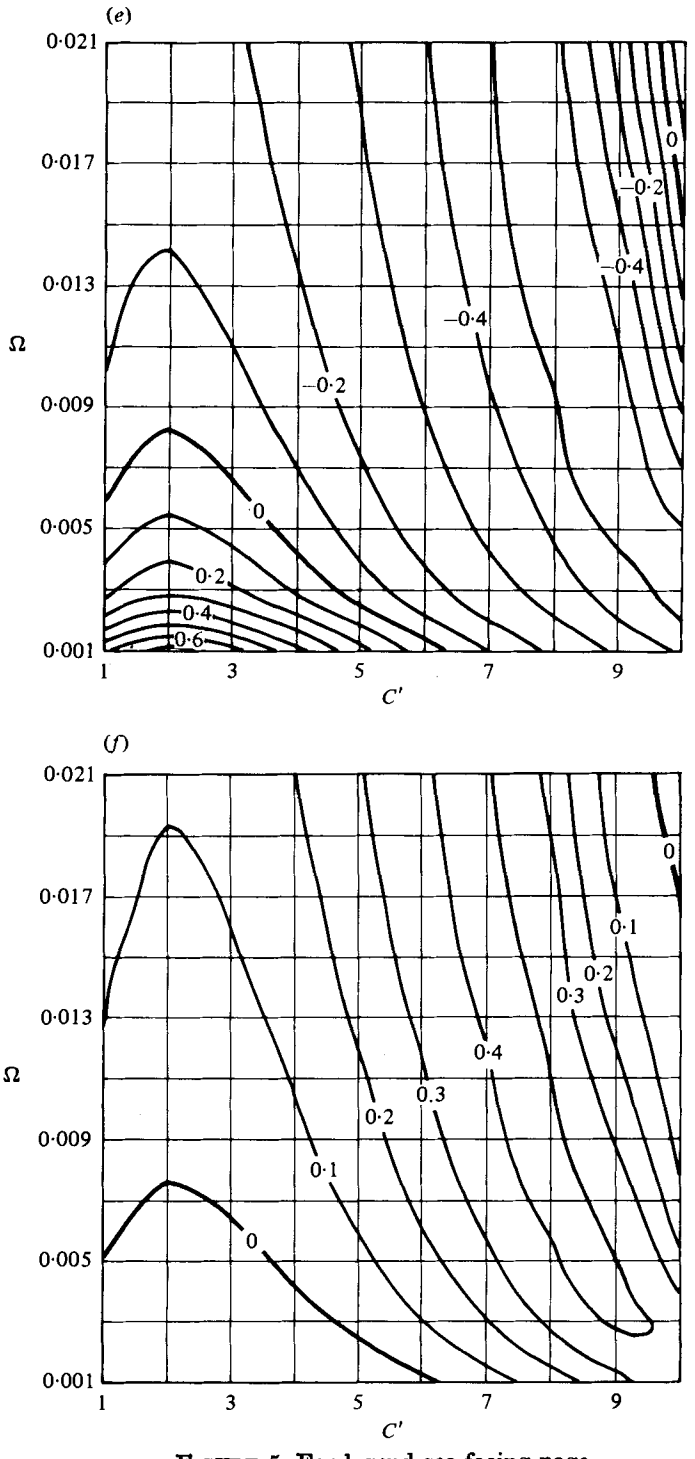

FIGURE 5. For legend see facing page.

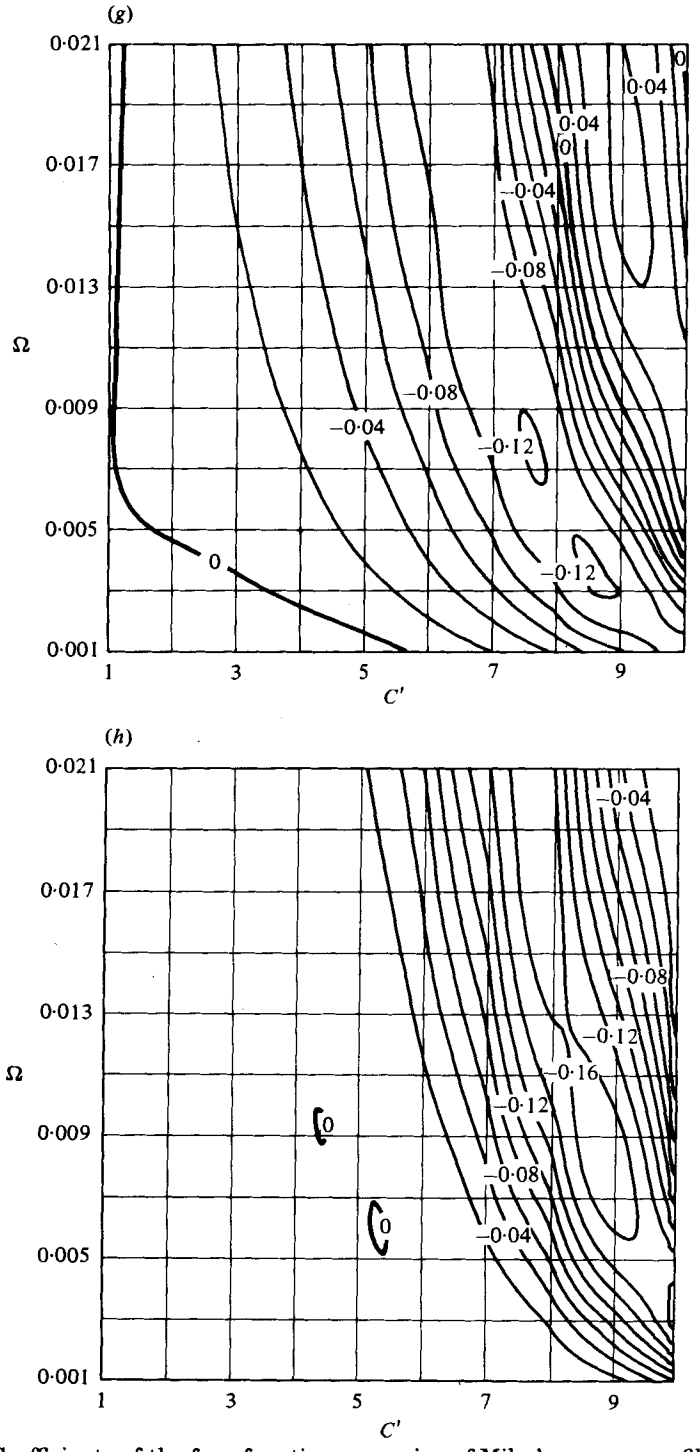

FIGURE 5. Coefficients of the four-function expansion of Miles' pressure profiles, $\hat{P}' = \Sigma_{j=1}^{4} a_j' \phi_j$. Panels (*a*), (*c*), (*e*) and (*g*) show the real parts of a_1' to a_4' respectively; while (*b*), (*d*), (*f*) and (*h*) show the corresponding imaginary parts. The curves are contours of constant Re $\{a_j'\}$ or Im $\{a_j'\}$. In some regions, intermediate contours (dashed curves) have been added to aid interpolation.

4. Applications

To reconstruct a theoretical profile such as those shown in figure 3, one reads the real and imaginary parts of the complex coefficients $a'_j(C', \Omega)$ from the corresponding contour plots and forms the sum

$$\hat{P}'(C', \Omega; h') = \sum_{j=1}^{4} a'_j(C', \Omega)\, \phi_j(h').$$

To the extent that the coefficients may be accurately determined from the plots, this four-term expansion is capable of representing the profile so precisely that, on the scale of figure 3, the reconstruction is indistinguishable from the original. Dimensional profiles are then given by

$$\hat{P}(U_*, z_0, \theta, \omega; z) = \sum_{j=1}^{4} a_j(U_*, z_0, \theta, \omega)\, \phi_j(k(\omega)\, z),$$

where

$$a_j(U_*, z_0, \theta, \omega) = U_1^2(U_*, \theta)\, \rho k(\omega)\, a'_j\left(\frac{C(\omega)}{U_1(U_*, \theta)}, \frac{g z_0}{U_1^2(U_*, \theta)}\right) \tag{4.1}$$

and the dependence on wind and wave parameters has been indicated explicitly. On the other hand, in dealing with experimental data of the form (1.3), the coefficients are allowed to be free parameters in a model for $\hat{P}$ (equation (2.6)); then using the model in (1.2) gives

$$E_{\zeta P}(U_*, z_0, \theta, \omega; z) = E_{\zeta^2}(\theta, \omega) \sum_{j=1}^{J} a_j^*(U_*, z_0, \theta, \omega)\, \phi_j(k(\omega)\, z), \quad J \leqslant 4.$$

The a_j are then fixed by fitting this model for $E_{\zeta P}$ in the least-squares sense to the available set of frequency cross-spectra $G_{\zeta P}$.

This completes the parametrization of the vertical dependence of $\hat{P}$ (and, hence, $E_{\zeta P}$). In practice, the fitting of this model to data of the form (1.3) requires that the dependence of the a_j on θ also be parametrized. Although this aspect of the model-fitting problem is peripheral to the present study, some comments seem appropriate to place the present work in perspective.

To take maximum advantage of the linearity of the proposed vertical structure model, the parametrization of the θ dependence should also be linear, in which case the integration over θ in (1.3) can be carried out. This suggests the expansion

$$a_j(U_*, z_0, \theta, \omega) = \sum_{m=1}^{M} b_{jm}(U_*, z_0, \omega)\, \sigma_m(U_*, z_0, \theta, \omega),$$

where σ_m is a member of a suitable basis function set. Then, fitting the model data

$$\tilde{G}_{\zeta P}(U_*, z_0, \omega; \mathbf{r}, z) = \sum_{j=1}^{J} \sum_{m=1}^{M} b_{jm}^*(U_*, z_0, \omega) \times \left\{ \int_0^{2\pi} d\theta\, E_{\zeta^2}(\theta, \omega)\, \sigma_m^*(U_*, z_0, \theta, \omega)\, e^{i\mathbf{k}(\theta, \omega)\cdot\mathbf{r}} \right\} \phi_j(k(\omega)\, z) \tag{4.2}$$

to the observed data $G_{\zeta P}$ in the least-squares sense reduces to solving a set of linear algebraic equations for the unknown complex coefficients b_{jm}. As with the z dependency, it is important to choose a basis function set capable of adequately approximating the

true distributions with a minimum number of terms in the expansion. This suggests turning again to theory for guidance; we could, for example, perform an empirical orthogonal function analysis of the a'_j values derived from Miles' theory to deduce the two-dimensional basis function set $\sigma'_m(C', \Omega)$; then, from (4.1),

$$\sigma_m(U_*, z_0, \theta, \omega) = U_1^2(U_*, \theta)\,\rho k(\omega)\,\sigma'_m\left(\frac{C(\omega)}{U_1(U_*, \theta)}, \frac{gz_0}{U_1^2(U_*, \theta)}\right).$$

The integral in (4.2) would then become

$$\int_0^{2\pi} d\theta \cos^2\theta E_{\zeta^2}\,\sigma'^*_m\, e^{i\mathbf{k}\cdot\mathbf{r}}$$

the factor $(U_*/\kappa)^2\rho k$ being absorbed into b_{jm}. Given the parameters of the experiment (U_*, z_0, and E_{ζ^2}), the integration range $0 < \theta < 2\pi$ corresponds at a given frequency ω to a specific curve in the (C', Ω) plane; the integral could then be evaluated numerically for each m and instrument displacement $\mathbf{r}$, leaving a set of linear, algebraic equations for the free parameters b_{jm}.

No analysis as elaborate as this has been justified by the data collected to date. Both Dobson (1971) and Elliott (1972), lacking directional discrimination in the designs of their experiment, assumed *a priori* that both wave and pressure fields were essentially unidirectional, which is equivalent in the notation of (4.2) to setting $M = 1$ and taking

$$E_{\zeta^2}(\theta, \omega)\,\sigma_1^* = E_{\zeta^2}(\omega)\,\delta(\theta)$$

(where $E_{\zeta^2}(\omega)$ is the surface wave frequency spectrum and $\delta(\theta)$ the Dirac delta function). Further, their observations were unable to resolve the separate influences of U_* and z_0, so that they chose a single parameter, the wind speed at 5 m elevation (U_5), to characterize the wind. Snyder *et al.* (1980), in analysing the most extensive data set yet collected on the pressure field above waves, chose for their linear analysis

$$\sigma_m = \left(\frac{U_5}{C}\cos\theta\right)^{m-1},$$

deeming their data still inadequate to sort out more than a one-parameter dependence on the wind profile. While characterizing the wind profile by U_5 makes a rigorous comparison of the experimental results with theory difficult, it is an experimentally unequivocal parametrization and yields a useful empirical representation of the atmospheric input to waves (for application to wave fore/hindcasting models, for example).

Ultimately, the value of our proposed model for the vertical structure of wave-induced atmospheric pressure depends on how well it reproduces real profiles with a minimum number of terms in the expansion. Until direct, model-independent determinations of the structure of real profiles have been achieved, the only accessible measure of model performance is the extent to which data of the form (1.3), observed at a few discrete values of z and $\mathbf{r}$, match the corresponding integral properties of the model. Error in these fits arises from many sources, including statistical variability in the observations, errors in the estimation of E_{ζ^2}, and shortcomings in the parametrization of the directional dependence of $\hat{P}$ as well as inadequacies in the vertical structure model, and it is difficult to identify that component due primarily to the

(*a*) Laguerre basis

	J		
M	1	2	3
3	0·0961	0·0855	0·0848
4	0·0857	0·0852	0·0845

(*b*) Miles empirical orthogonal function basis

	J		
M	1	2	3
3	0·0863	0·0857	0·0851
4	0·0863	0·0853	0·0859

J = number of terms in the vertical structure expansion of $\hat{P}$.
M = number of terms in the directional expansion of $\hat{P}$.

TABLE 3. Proportional variance of model fits to the field data of Snyder *et al.* (1980)

latter. Some indication is provided by the analysis of Snyder *et al.* (1980), who tabulated the proportional variance (mean-square difference between modelled and observed cross-spectra normalized by the product of the corresponding observed autospectra) of fits to a total of six data sets acquired with an array of six microbarographs and five wave gauges. The directional properties of $\hat{P}$ were modelled using the σ_m indicated above, while the vertical structure expansion used the empirical orthogonal functions developed here and an alternative set of non-orthogonal functions

$$\phi_j = (z')^{j-1} e^{-z'}$$

(related to the Laguerre polynomials). When only one term in the vertical structure expansion and three terms in the directional expansion are used, the empirical orthogonal function model seems clearly superior (see table 3), implying in this case that the experimental profiles more closely resemble the fundamental empirical orthogonal function of figure 4 than they do e^{-kz}; this is consistent with Elliott's observations as discussed in §3. Moreover, retaining additional terms in the empirical orthogonal function expansion fails to make a significant improvement, indicating that the residual variance in the fits is already dominated by sources unrelated to the $\hat{P}$ model. The Laguerre expansion, on the other hand, is improved by adding an additional term in either expansion, after which differences between the two model choices become negligible. Though the discrimination of these comparisons is obviously poor, they do provide additional support for the use of the empirical orthogonal function basis for this type of analysis.

5. Summary and conclusions

The spectral quantity defining the rate at which energy is transferred from wind to waves is the surface-elevation/atmospheric-pressure directional cross-spectrum $E_{\zeta P}$, evaluated at the mean water surface. Experimentally, it is very difficult to measure the atmospheric pressure at this level in the presence of waves, but by making observa-

tions of surface elevation and air pressure at various horizontal and vertical positions, certain integral moments of $E_{\zeta P}$ can be estimated; $E_{\zeta P}$ may then be estimated by fitting a parametrical model to the observations. To assure statistical significance, the model must be efficient at representing the observations with a minimum number of free parameters; moreover, the vertical structure of the model is critical if its value at the mean water surface is to accurately approximate the true (but experimentally inaccessible) value of $E_{\zeta P}$ at $z = 0$. Using the theory of Miles (1957) for guidance, we have designed a parametrical model for this vertical dependence in the form of a linear expansion in a set of empirical orthogonal functions derived from a set of theoretical pressure profiles. As a by-product of the model development, we have produced contour plots of the coefficients of a four-function expansion of the same set of theoretical profiles. These, along with the corresponding empirical orthogonal functions, provide a graphical means of reconstructing the theoretical wave-induced pressure field.

The empirical orthogonal function expansion is capable of representing all of the Miles theoretical profiles with great accuracy using only a few terms and exhibits sufficient flexibility to reproduce profiles derived from alternative theories with nearly equal efficiency. It seems likely, therefore, that this expansion will be highly efficient at reproducing pressure profiles existing in nature. It has been successfully used to analyse a body of experimental data on wave-induced atmospheric pressure fluctuations by Snyder *et al.* (1980).

REFERENCES

Conte, S. D. & Miles, J. W. 1959 *J. Soc. Indust. Appl. Math.* **7**, 4.

Davis, R. E. 1969 *J. Fluid Mech.* **36**, 337.

Davis, R. E. 1970 *J. Fluid Mech.* **42**, 4.

Davis, R. E. 1976 *J. Phys. Oceanog.* **6**, 3.

Dobson, F. W. 1971 *J. Fluid Mech.* **48**, 1.

Elliott, J. A. 1972 *J. Fluid Mech.* **54**, 3.

Gent, P. R. & Taylor, P. A. 1976 *J. Fluid Mech.* **77**, 1.

Hasselmann, K. 1967 *Proc. Roy. Soc.* A **299**, 77.

Hasselmann, K. 1968 Weak interaction theory of ocean waves. In *Basic Developments in Fluid Dynamics*, vol. 2 (ed. M. Holt), p. 117.

Lin, C. C. 1967 *The Theory of Hydrodynamic Stability.* Cambridge University Press.

Long, R. B. 1971 Ph.D. thesis, University of Miami, Florida.

Lorenz, E. N. 1956 Empirical orthogonal functions and statistical weather prediction. *Statistical Forecasting Project, Rep.* no. 1. Dept. Meteorology, MIT.

Meksyn, D. 1961 *New Methods in Boundary Layer Theory.* Pergamon.

Miles, J. W. 1957 *J. Fluid Mech.* **3**, 185.

Moore, D. 1974 *MODE Hot Line News*, **67**.

Phillips, O. M. 1966 *The Dynamics of the Upper Ocean.* Cambridge University Press.

Smith, W. L. & Woolf, H. M. 1976 *J. Atmos. Sci.* **33**, 7.

Snyder, R. L. 1974 *J. Mar. Res.* **32**, 3.

Snyder, R. L., Dobson, F. W., Elliott, J. A. & Long, R. B. 1980 Array measurements of atmospheric pressure fluctuations above surface gravity waves. *J. Fluid Mech.* (to appear).

Townsend, A. A. 1971 *J. Fluid Mech.* **55**, 4.

Winant, C. D., Inman, D. L. & Nordstrom, C. E. 1975 *J. Geophys. Res.* **80**, 15.